ELSEVIER

Surface Science 376 (1997) 133–150

surface science

Nucleation and growth of silver films on a rhenium (0001) surface: a combined STM and LEED study

M. Parschau, D. Schlatterbeck, K. Christmann *

Institut für Physikalische und Theoretische Chemie der Freien Universität Berlin, D-14195 Berlin, Germany

Received 6 October 1995; accepted for publication 12 November 1966

Abstract

Ag thin films on an Re(0001) surface prepared by vapor deposition at 300, 400 and 600 K were studied by means of low-energy electron diffraction (LEED) and scanning tunneling microscopy (STM). At $T=300$ K, Ag atoms nucleate heterogeneously at every monoatomic Re step edge and diffusion-limited aggregation leads to dendritic Ag islands, which coalesce to a porous film near the monolayer. Still larger coverages result in more densified Ag layers, due to enhanced interlayer mass transport facilitated by low Schwoebel barriers for second-layer Ag islands. At $T>400$ K Ag atoms nucleate only at *every second* monoatomic step, indicating a preference for the formation of (111) microfacets and a pronounced mobility of Ag atoms perpendicular to the step edges. Compared to the 300 K situation, even more compact and better ordered layers are formed, resulting in a clear layer-by-layer growth (of Frank-van-der-Merwe type), but with a strongly layer-dependent morphology. Ag grows pseudomorphically in the first layer as indicated by misfit dislocation domains, uniaxially expanded lines of Ag atoms form in the second layer and STM moiré structures (paralled by appropriate LEED superstructures) appear for the third and fourth layer (at $T\geq 400$ K). In the fifth layer the 4.7% Ag–Re lattice misfit is practically accommodated and clear epitaxial growth of Ag(111) crystallites occurs.

Keywords: Epitaxy; Low energy electron diffraction (LEED); Metal film growth; Nucleation; Rhenium; Scanning tunneling microscopy; Silver

1. Introduction

The currently strongly increasing number of publications dealing with thin film growth and nucleation phenomena reflects the sustained interest in the morphology of thin films and the related physical and chemical properties of these materials. On the other hand, it can be considered a consequence of the power of today's scanning tunneling microscopy techniques which allow imaging of surface structure and morphology with atomic resolution almost routinely. Even more powerful are thin film studies when they are combined with conventional surface-sensitive techniques such as LEED, Auger electron spectroscopy (AES), X-ray photoelectron spectroscopy (XPS) or temperature-programmed thermal desorption (TPD), since these supplementary methods often allow a correlation between, for example, surface structure and binding energies, work function effects, conductivity, optical reflectivity, chemical composition, catalytic activity, etc.

We were interested in the nucleation and growth behavior of silver thin films deposited on a rhenium(0001) surface. This system may represent a

* Corresponding author. Fax: +49 30 8386612.

0039-6028/97/$17.00
PII S0039-6028(96)01303-9

chemically interesting bimetallic model catalyst, somewhat similar to the previously investigated Cu/Ru(0001) [1–6], Au/Ru(0001) [7] and Ag/Ru(0001) systems [8,9]. Bimetallic systems of this kind can exhibit a peculiar catalytic selectivity for certain hydrocarbon synthesis and/or decomposition reactions [10–12]. Note that the noble metals Cu, Ag and Au do not form bulk alloys with Re [13], which should make nucleation and growth studies of Ag thin films with this substrate less complicated than in cases where interlayer diffusion and alloying effects occur; examples of this are, among others, Cu on Pd [14], Ni on Cu [15] or Al on Ru [16,17].

The choice of Re as a substrate was motivated by several reasons. First, it is an important constituent of reforming catalysts [18] and the dilution and/or inhibition of active surface sites by an inert noble metal such as silver could lead to particular catalytic properties because electronic (ligand) and geometric (ensemble) effects [19] may provide a particular selectivity and/or activity increase. Second, Re(0001) is a close-packed surface with hexagonal symmetry (hcp structure) and only recently there appeared reports in the literature in which noble metal growth was followed on these crystallographically smooth surfaces, with ruthenium(0001) given as a particular example [1–9,20–24].

Re(0001) can be considered a very smooth surface on the atomic scale. In a recent STM study dealing with cobalt thin film growth onto Re(0001) we determined the mean corrugation amplitude of this surface to be less than 0.1 Å [25] and it was an interesting task to study the nucleation and growth behavior of a noble metal with low melting point and expected high mobility on such a surface. By appropriate chemical cleaning, sputtering and annealing we were able to prepare homogeneous surfaces which were characterized by very wide atomically smooth terraces (width $\geq$ 1000 Å). At a few points on the surface there also existed some zones with a rather more perturbed character showing step bunching, with sequences of quite narrow steps of mostly monoatomic height (width $\leq$ 100 Å) [25,26].

In the STM investigations of the Cu and Au on Ru(0001) systems pronounced fractal growth features were observed [20–24] indicating significant kinetic limitations in the noble metal thin film growth; these effects were much more prominent for Au than for Cu deposition [22]. Nevertheless, both noble metals clearly wetted the Ru surface and exhibited a pronounced spreading on the surface to form relatively homogeneous layers of monoatomic thickness. Another important issue concerns the temperature dependence of the nucleation and growth features. For a variety of heteroepitactic metal-on-metal systems evidence of site exchange processes, interlayer diffusion and/or surface alloy formation has been reported; these effects are most prominent at elevated temperatures. Examples of this kind of "chemical" interactions are, among others, provided by the Co-on-Re(0001) system [25,26] and (less pronounced) by the Ag-on-Pt(111) system [27].

In the following, we will describe the body of our STM results obtained with Ag-on-Re(0001) between 300 and 600 K, supplemented by LEED. A full account of our combined XPS, AES, LEED, TPD and $\Delta\Phi$ results will be given elsewhere [28].

2. Experimental

All experiments were carried out in a stainless-steel ultra-high vacuum (UHV) chamber equipped with the standard facilities for preparing and characterizing a clean metal surface, among others a four-grid electron optics for LEED and AES. A UHV tunnel microscope (rasterscope 3000, DME) allowed, after appropriate tip and sample handling, atomic resolution. By means of a wobble-stick (WA technology) the sample could be transferred between the UHV manipulator and the tunnel microscope. In order to damp harmful vibrations, the whole apparatus rested on commercial shock absorbers (Newport). Typically, the tunnel microscope was operated at room temperature in the constant current mode with tunnel currents between 0.1 and 3 nA and bias voltages between +1 and +400 mV.

A combined pumping system consisting of a 270 l s^{-1} turbomolecular pump and a 450 l s^{-1} ion getter pump (Varian) provided a base pressure of 10^{-10} mbar; even during prolonged Ag depos-

ition from a Knudsen cell (see below) the chamber pressure remained in the low 10^{-10} mbar range.

The Re(0001) sample of 5N purity consisted of a disk ~ 1 mm thick and ~ 8 mm in diameter. It was mounted on a conventional sample manipulator, which allowed in situ positioning as well as heating by electron bombardment ($T_{max} \approx 2500$ K). The sample temperature was measured using an Re/WRe thermocouple spot-welded to the sample holder, which was in excellent mechanical and thermal contact with the Re crystal. Accordingly, there were only very small temperature differences between the thermocouple/sample holder and the actual sample, as repeatedly controlled by optical pyrometry.

The main cleaning procedure of the Re sample consisted of a few minutes heating in oxygen ($P_{O2} \approx 2 \times 10^{-8}$ mbar) at $T = 1100$ K, followed by a short heating to 1500 K in a hydrogen atmosphere ($P_{H2} \approx 2 \times 10^{-7}$ mbar) and a flash to ~ 2300 K in order to remove residual oxygen. No Ar ion sputtering was employed in order not to damage the Re surface. The cleaning procedure was continued until there were no longer sulfur, carbon and oxygen signals detectable in AES, and the LEED pattern exhibited bright and sharp diffraction spots on a low background.

The evaporation of silver was performed from a commercial thermal effusion (Knudsen) cell (WA technology) containing a graphite crucible loaded with ultrapure (5N) Ag wire (Goodfellows) at a temperature of ~ 1000 K, where the vapor pressure of Ag is sufficiently high to achieve deposition rates of a few monolayers per hour. From AES we deduced that (after appropriate outgassing of the source) the as-deposited Ag films were very clean; the sulfur, carbon or oxygen contaminations mentioned above could not be detected.

3. Results and discussion

3.1. General remarks

After appropriate cleaning and annealing the Re(0001) surface showed the expected hexagonal LEED pattern with sharp diffraction spots on a low background, indicating a chemically clean and crystallographically well-ordered substrate surface. (The chemical cleanliness was also established from AES and XPS measurements reported in more detail elsewhere [28].) On Re surfaces of this kind we deposited Ag films of various thicknesses either at room temperature or at elevated temperatures ($400\ \mathrm{K} < T < 600$ K); in some experiments the 300 K films were also annealed to higher temperatures ($T > 400$–700 K). The standard deposition rate was ~ 5 nominal monolayers per hour. Actual silver coverages Θ were estimated from a direct inspection of large-scale tunnel images, whereby we define Θ as usual as the number of Ag surface atoms related to the topmost Re surface atoms ($\Theta = 1$ then means 1.515×10^{19} atoms m^{-2}); the relative amounts of deposit could be deduced from TPD peak integrals $\int P\,\mathrm{d}t$, Ag-induced work function changes (in the submonolayer range) and XPS signal intensities with high accuracy [28].

We have organized the presentation of our results as follows. First, the Ag films prepared at room temperature will be described; their growth is largely determined by *kinetic* effects. Thereafter we will present the data obtained for the films deposited at elevated temperatures ($T \geq 400$ K), which are rather dominated by *thermodynamics*.

3.2. Ag deposition at room temperature: the role of kinetic limitations

3.2.1. Low-energy electron diffraction

The first noticeable changes in the LEED pattern occur after deposition of about two tenths of a monolayer (ML) ($\Theta_{Ag} \approx 0.2$) in that the initially very low background intensity rises, although without any indications of a new superstructure, and, accordingly, the Re diffraction spot intensity decreases somewhat. As more Ag is deposited, the diffuse background intensity continues to rise and then remains at a certain level, while the Re-derived hexagonal (1×1) LEED spots are still recognizable (although weak) up to a total coverage of ~ 4 ML of Ag. It was not possible to observe a new Ag-induced LEED superstructure under these conditions – any such patterns were only obtained after Ag deposition onto the heated Re substrate or after annealing of the 300 K films to 400–500 K and 700 K, respectively, cf. Section 3.3.1. However, massive silver deposition to a total of more than 5 or 6 monolayers finally produces a LEED pattern

(although with relatively diffuse spots) in which a hexagon of "extra" spots is inscribed in the hexagon of the Re(1 × 1) reflexes, which points to a final growth of Ag crystallites with their inherent (Ag(111)) lattice constant.

The room temperature LEED data suggest, for coverages up to approximately four Ag monolayers, fairly disordered Ag films with an appreciable concentration of holes and other defects; the high diffuse background indicates a very ramified growth of the Ag crystallites at least within the first couple of layers, a conclusion which can also be drawn from the STM data to be reported next. Whether or not there occurs pseudomorphic growth in the first and/or second Ag layer cannot be deduced with certainty from the room temperature LEED experiments alone. Normally a pseudomorphic growth would *not* cause a marked increase of the diffuse background since the deposit atoms exhibit the same translational symmetry as the substrate lattice. However, for pseudomorphic aggregates with fractal character their very rough edges [29,30] can represent strong scattering centers for low-energy electrons, which may significantly contribute to the disordered background. As will be shown later, just this situation seems to hold in the present case since we have hints from our STM data to pseudomorphic growth, at least in the first Ag layers. Among others, this statement rests on the observation of (i) uncorrugated homogeneous Ag films in the first monolayer and (ii) misfit dislocation domains for a two-Ag layer film deposited at room temperature, as will be demonstrated in the following section.

3.2.2. Scanning tunneling microscopy

The clean and well-annealed Re(0001) surface is surprisingly homogeneous and flat; terrace widths of more than 10 000 Å are by no means unusual. To give an example, we present in Fig. 1a a larger-scale scan showing a monoatomic Re terrace with a width of ~500 Å. STM images with atomic resolution, cf. Fig. 1b, clearly show the hexagonal close-packing of the (0001) orientation with its characteristic Re–Re distance of 2.76 Å and the extremely small corrugation of less than 0.1 Å.

In order to examine the very first stages of Ag nucleation and condensation, we have deliberately chosen a region of the Re surface which exhibits a high local step density. In Fig. 2a we show a large-scale detail with a sequence of three (bent) monoatomic steps, each on average more than 5000 Å wide, after deposition of ~0.1 ML of silver at 300 K. Clearly, the Ag atoms nucleate *exclusively* at the step edges under these conditions, where they form irregularly shaped small aggregates which reach far out onto the flat terraces. The average distances of the individual nuclei formed at a given step edge are thereby fairly large, which means that the Ag atoms do not really *wet* the step edges (in this case one-dimensional "lines" of Ag atoms would be formed along these edges) but incidentally hit the steps and stick there. This points to a pronounced kinetic limitation in the diffusivity of the Ag atoms, especially near the steps (and the edges of Ag nuclei). The irregular and fairly porous shape of the individual Ag aggregates is striking; the "arms" of the respective Ag networks are not much wider than 50 Å and large "cavities" are formed due to the totally undirected growth. This behavior is in contrast to our previous room temperature STM investigation of the growth of Co on a Re(0001) surface [25]. With this system, we found triangular-shaped dendritic islands, with the edges of the triangles oriented parallel to the main symmetry directions of the hexagonal Re(0001) substrate. No such "easy"

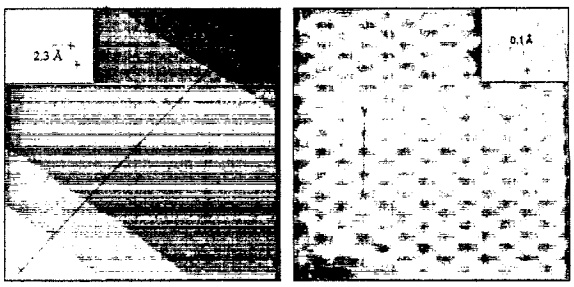

Fig. 1. (a) Large-scale STM scan (800 Å × 800 Å) showing a terrace/step combination of five monoatomic Re terraces, the large terrace with a width of ~500 Å is actually free of defects (tunnel current $I = 0.35$ nA; bias voltage $U = 130$ mV). (b) STM image of the Re(0001) surface with atomic resolution (33 Å × 33 Å) showing the hexagonal close-packed symmetry with its characteristic Re–Re distance of 2.755 Å and the extremely small corrugation of less than 0.1 Å ($I = 1.36$ nA; $U = 3$ mV).

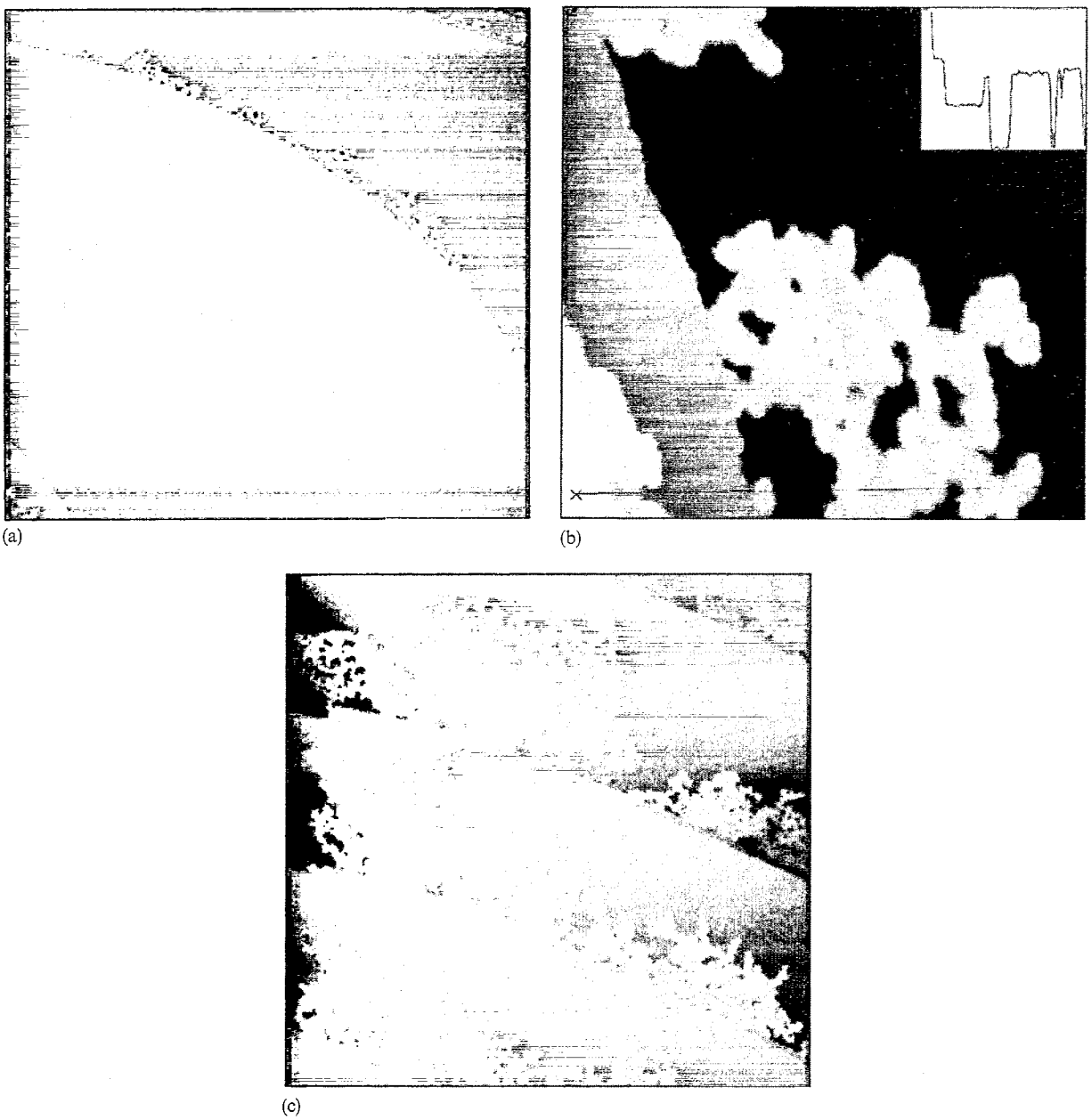

Fig. 2. (a) Large-scale image of the Re(0001) surface (12 000 Å × 12 000 Å) after deposition of 0.1 ML of Ag at 300 K showing a sequence of three (bent) monoatomic steps, each on average more than 5000 Å wide, with Ag nuclei formed at the step edges ($I=0.1$ nA; $U=417$ mV). (b) STM image (2000 Å × 2000 Å) of a stepped region of the Re surface covered with ~0.1 ML Ag at 300 K, including a height-contour plot along the indicated line that proves that the imaging height of a monoatomic Ag film exceeds somewhat the monoatomic step height of an Re edge, with the height of the Ag island being 3.2 ± 0.4 Å and that of the Re step $\sim2.3\pm0.4$ Å ($I=0.12$ nA; $U=470$ mV). (c) STM image (12 000 Å × 12 000 Å) of a stepped region of the Re(0001) surface covered with ~0.3 ML of Ag at 300 K. Note the growth of extended but very porous Ag islands nucleating at every step edge and extending far out onto the flat terraces. Apparently, no particular growth direction is preferred ($I=0.1$ nA; $U=100$ mV).

growth direction is recognizable with Ag on Re, which points to a largely diffusion-limited aggregation mechanism. This kind of aggregation is often observed for metal-on-metal epitaxy and indicates non-equilibrium growth that is limited by the diffusion of adatoms around the perimeter of a given nucleus. Appropriate theoretical models (DLA model) were developed by Witten and Sander [31,32] and Meakin [33,34]. Experimental verifications have been reported, among others, by Hwang et al. for Au growth on an Ru(0001) surface [21,35]. While the plain DLA model should lead to fractal arms of atomic width, our results rather yield arms about 50 Å wide, which points to a more *relaxed* DLA mechanism where arriving atoms are still able to reach energetically favorable positions, at least on a *local* scale. Examples for this type of growth have been reported by Chambliss et al. [29] and by Röder et al. [30], and we refer to their publications for further details.

As the Ag coverage increases (within the submonolayer range) there is still no evidence of any homogeneous nucleation on the Re terraces. This means that the average diffusion length of the adatoms is larger than the mean distance between two adjacent substrate steps and the number of Ag atoms on the terraces is more rapidly depleted (via diffusion to and nucleation at the step edges) than Ag atoms impinge on the terraces from the vapor phase.

Another important point concerns the actual *height* of the silver islands. For its exact determination it is again advantageous to focus on a region of the Re surface which exhibits regular monoatomic steps with their well-known height of ~ 2.25 Å and to compare it with the STM imaging height of the Ag island. Fig. 2b shows a respective STM image of such a stepped part of the Re surface covered with ~ 0.1 ML Ag at 300 K, including a height-contour plot along the indicated line. Taking into account all sources of errors (which amounts to a total uncertainty of $\sim 15\%$), we arrive at an Ag island height of $\sim 3.2 \pm 0.4$ Å, which is considerably larger than the interlayer spacing of Ag(111) ($d_{Ag(111)} = 2.72$ Å). Increased STM imaging heights are well established for metallic monolayers, e.g. for the systems Ag-on-Au(111) [29] or Ag-on-Pt(111) [36] as well as for Cu-on-W(110) [37] (for reasons which must primarily be sought in the imaging of the density of electronic states at the Fermi level). All in all, we are confident that the measured height of the Ag islands can be interpreted as the *monoatomic* height. This assumption is further supported by recent work function change measurements with the Ag-on-Re(0001) system by Schlatterbeck et al. [28]. These measurements revealed, for the monolayer coverage range, a decrease of $\Delta\Phi$ to a value which is almost 700 meV lower than the work function of the clean Re substrate. A decrease of the work function, on the other hand, will give rise to an increased tunnel current and in the constant-current mode the STM tip will be somewhat removed from the surface, resulting in a too-large imaging height for the Ag ad-islands.

As the silver deposition is continued, the Ag nuclei grow by random condensation of Ag atoms at the perimeters of the islands. In this way, a loose network of islands is formed, a typical example being shown in Fig. 2c for an ensemble of approximately nine Re terraces with periodically alternating widths. Although this network becomes gradually filled and densified as Θ_{Ag} increases, a sudden coalescence as it was reported, for example, for Fe films on W(110) [38], does not take place. Rather, the film spreads continuously across the flat terraces and finally covers them entirely, thereby retaining its quite porous, or even "fluffy", character. As the coverage approaches the full monolayer, coalescence increasingly takes place and leads to films which are more compact but still exhibit numerous pores.

We then gradually increased the Ag coverage further to a total of more than 4 monolayers. The transition from the first to the second monolayer occurs only once the first layer is almost completed, which points to an appreciable interlayer mass transport. Ag atoms which arrive on top of the first layer are mobile enough to either reach a vacancy in the first layer or to push atoms of the first layer aside. No Ag nuclei are formed in the second layer until the first layer is practically completed. The next series of STM images (Figs. 3a–3d) illustrates how the silver deposit grows to a thickness of ca. 4 monolayers. First we display in Fig. 3a a detail of the Re surface with a high

density of steps after deposition of ~1.3 Ag monolayers. On some of the terraces the second-layer nuclei have already grown to extended Ag islands, while one-monolayer films still exist on adjacent terraces. This kind of locally inhomogeneous Ag coverage could also be found in the submonolayer coverage range, especially in regions with a high local step density. We may conclude that at least some Ag atoms are able to overcome the activation barrier for diffusion at the descending step edges, which explains, along with asymmetries in the flux across adjacent steps, the fairly pronounced differences in the local Ag coverage. The aforementioned asymmetries in the flux across the steps points to the build-up of a repulsive activation barrier right at the link between the Ag film and an adjacent substrate step which impairs the transport of Ag atoms via the formation of a fringe of Ag atoms right at the step edge. Another hint to this repulsive barrier is provided by the observation that a coalescence of Ag films of different thickness formed on adjacent terraces *does not occur*; rather the individual layers remain separated by sharp lines right at the positions of the former substrate steps. This situation is depicted in Fig. 3b, which images a large area (1.6 μm × 1.6 μm) of the Re surface after deposition of ~1.8 Ag monolayers. The contours of a central terrace (which is, for the most part, covered with a second-layer Ag film, on top of which even dendrites of the third layer begin to form, cf. in the lower left corner) can easily be identified as the former steps of the Re substrate.

Another observation deserves attention. We have already emphasized the very dendritic growth forms of the Ag islands in the first and second layer that led to a very porous structure of the Ag films. This growth behavior continues well into the third-layer coverage regime as Fig. 3c demonstrates for a slightly stepped part of the Re surface. Even in the third layer the Ag islands maintain this very porous and fractured morphology. It is not until the fifth Ag layer forms that the diffusive mobility of the Ag adatoms along the edges of the islands becomes sufficiently large that the Ag islands can take on a much less fractured and more compact shape, as demonstrated in Fig. 3d. On the other hand, one can also realize that the three- and four-monolayer films grown at 300 K exhibit an increasing overall roughness, which demonstrates that the growth at 300 K is largely dominated by kinetic effects. While the first- and second-layer films can almost grow to a complete monolayer, there coexist up to three individual incomplete layers at larger thicknesses and we must assume that the interlayer mass transport is somewhat hindered under these conditions, compared to the first-layer situation.

An effective interlayer mass transport only for very thin films indicates that the energy barriers located at the edge of a silver island (known as Schwoebel barriers [39]) are quite small as long as only a single Ag monolayer has been deposited on the Re substrate; they do not prevent the second-layer Ag atoms from reaching vacant positions in the first layer. It has become apparent that the height of these diffusion barriers is strongly dependent on the *structure* of the underlying layer. While for a clean Ag(111) surface the height of the Schwoebel barrier was determined to be 120 ± 15 meV [40] and 150 ± 20 meV [41], these values are substantially reduced, namely to merely 30 ± 5 meV, if Ag islands grow on top of a Pt(111) surface, and a correlation between the barrier height and the degree of compression of the Ag atoms is suggested [40]. If this concept is transferred to the Ag/Re(0001) system and it is taken into account that a compressed pseudomorphic first layer is formed for this system too (cf. Section 3.3), one could understand why the roughness of the room temperature films increases with thickness.

After the description of the nucleation and more "global" growth behavior we will now turn to another quite important point which is concerned with the "adsorption" of individual Ag atoms on the Re surface and further microscopic details of the heteroepitactic growth, especially the problem of how the lattice misfit between Ag and Re can be overcome. In the foregoing section we have seen that the diffusion and overall growth of Ag is largely determined by kinetics, at least at room temperature. Therefore, the formation of stable equilibrium structures with long-range order is very unlikely under these conditions. Unfortunately, we did not succeed in obtaining STM images with atomic resolution from our Ag films deposited at 300 K, in contrast to the experiments at elevated temperatures, cf. Section 3.3. It is

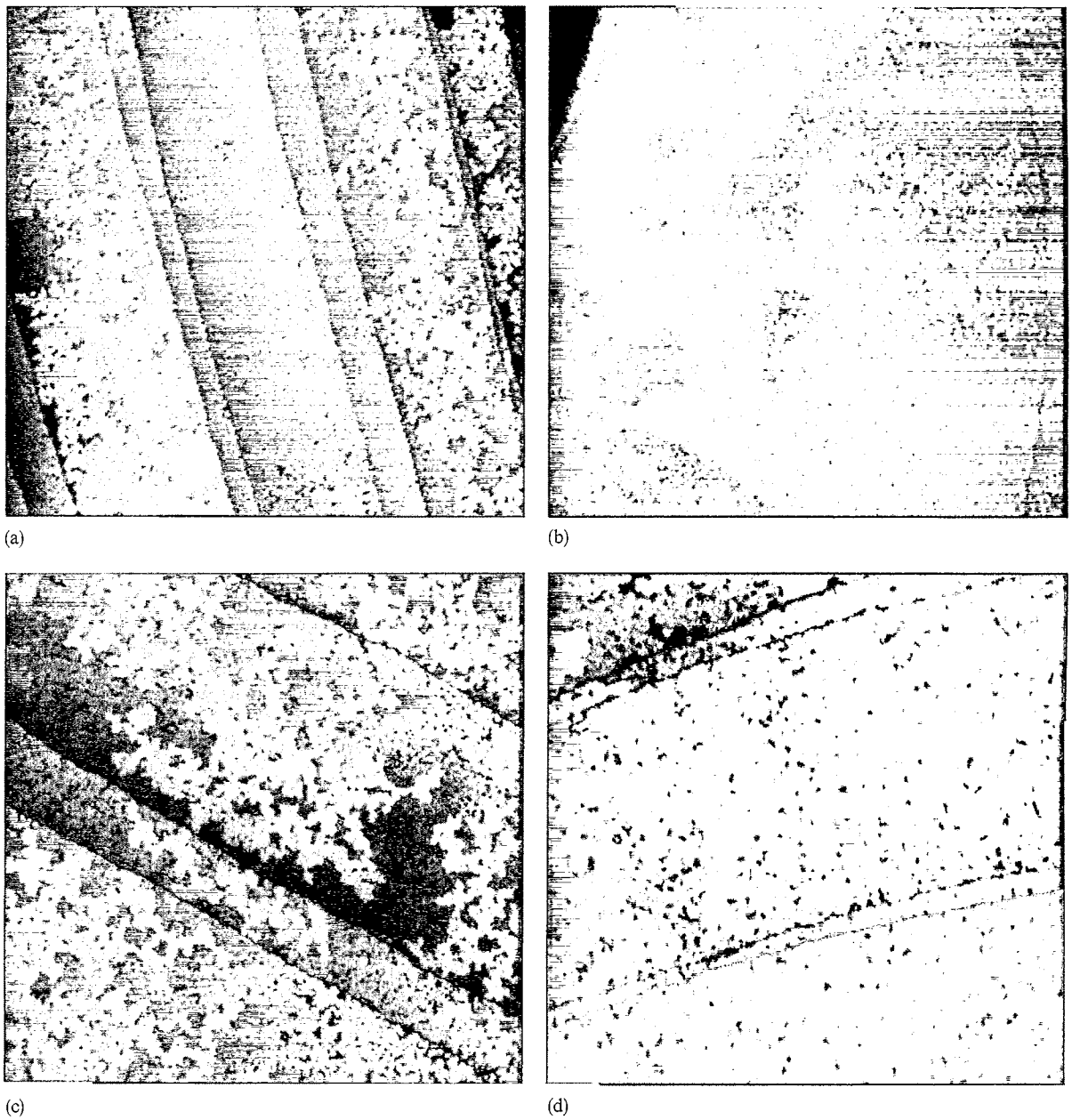

Fig. 3. (a) Stepped part of the Re(0001) surface covered with $\Theta \approx 1.3$ ML Ag at 300 K (850 Å × 850 Å). This STM image points to pronounced differences in the local Ag coverage: on some of the terraces the second-layer nuclei have grown to extended islands, while single monolayer films still exist on adjacent terraces ($I = 0.22$ nA; $U = 80$ mV). (b) STM image (16 000 Å × 16 000 Å) of an extremely wide terrace of the Re surface covered at 300 K with ~1.8 nominal Ag monolayers. The large central terrace is completely covered with an Ag monolayer on top of which a very large porous second-layer Ag island has grown. Near the right-hand edge of the photograph can be seen a long slightly bent line which corresponds to the trace of a former terrace that is not levelled off by the deposited silver. Furthermore, Ag islands with strongly fractal shape (in the lower left corner) indicate the beginning of growth of Ag atoms in the third layer; note that these islands nucleate on the flat parts of the terraces and, hence, prove homogeneous

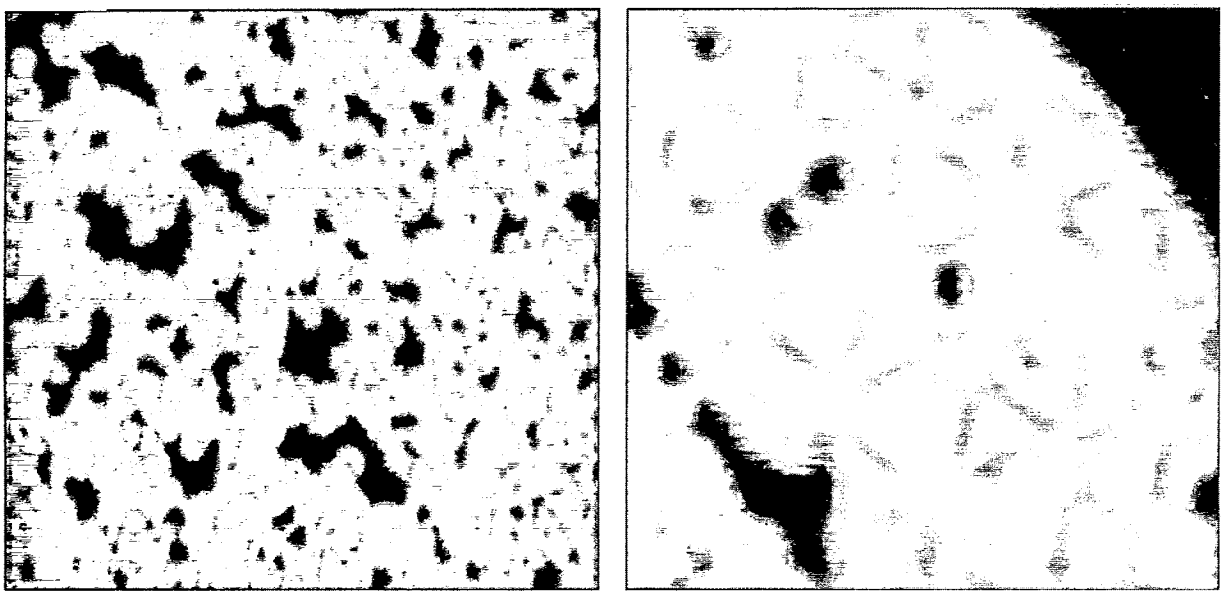

(a) (b)

Fig. 4. (a) 660 Å × 660 Å detail from a ~2 ML Ag film deposited at 300 K onto an Re(0001) surface that exhibits a peculiar surface morphology with a network of grooves ~0.6 Å deep running across the film and separating small triangular or hexagonal areas (mean diameter ≤ 30 Å) that we identify as Ag crystallites with different stacking sequence (hcp vs. fcc); so-called "misfit dislocation" domains ($I = 0.2$ nA; $U = 84$ mV). (b) Detail of an STM image (300 Å × 300 Å) of a three monolayer Ag film deposited at 300 K showing the misfit dislocation structure more clearly. Again there appear triangular and/or hexagonal depression lines ca. 0.3 Å deep and roughly 20–30 Å wide. We further emphasize that the Ag domains of a given stacking sequence (hcp or fcc) are absolutely *flat*, without any indications of a surface corrugation ($I = 0.22$ nA; $U = 87$ mV).

therefore difficult to conclude on the local Ag "adsorption-site" geometry or on possible long-range order effects within the Ag layers grown at 300 K. In Section 3.2.1 we addressed the problem of pseudomorphical growth. Figs. 4a and b show STM images of two- and three-monolayer Ag films, respectively, grown on a flat terrace of the Re(0001) surface. Both images clearly exhibit triangular networks (or patterns) of depression lines ca. 0.3 Å deep and roughly 20–30 Å wide. Furthermore, both films are absolutely *flat*; there are no indications of corrugation effects. These features point to a pseudomorphic growth for the following reason. In the very first layer, Ag atoms preferentially occupy the threefold coordinated sites provided by the Re substrate lattice. As this pseudomorphic layer becomes "buried" by the second and third Ag layer, the delicate balance between misfit energy and lateral Ag–Ag interaction energy changes and apparently produces misfit dislocation domains which are actually imaged in Fig. 4. Because of the Ag layer(s) deposited on top of the pseudomorphic film, the very first layer is subjected to additional tensile stress and apparently relaxes into domains ca. 20–30 Å wide in which the bottom layer Ag atoms are

nucleation of Ag on Ag ($I = 0.22$ nA; $U = 300$ mV). (c) The Ag islands maintain a fractal shape up to the growth of the fourth layer, as this STM image (420 Å × 420 Å) of a stepped region of the Re(0001) surface, covered with ~3.3 ML Ag illustrates. Note also the still fairly porous character of the third Ag layer; the dendritic islands represent the beginning of growth in the fourth layer ($I = 0.12$ nA; $U = 87$ mV). (d) STM image (360 Å × 360 Å) of a stepped part of the Re(0001) surface covered with ~4 ML Ag at room temperature. On top of the (still porous) fourth Ag layer, islands of the fifth layer can be distinguished whose shape is much more *compact* and indicates that the growth situation more and more resembles the Ag-on-Ag condensation. Also note that not more than three monolayers are "open" at the same time for a given stage of the growth ($I = 0.14$ nA; $U = 99$ mV).

located in threefold coordinated Re sites with either local face-centered cubic (fcc) or hcp symmetry. The observed depressions then arise whenever a site symmetry change between adjacent domains occurs. The *flatness* of the films thereby suggests that they are still pseudomorphic because otherwise a noticeable undulation of the top-layer film(s) should arise (which is *not* observed) due to the lattice misfit between the first (still pseudomorphic and, hence, compressed) layer and the (relaxed) second- and third-layer films. The observed misfit dislocation domains represent a kind of a typical response of a heteroepitactic system to relieve the interlayer strain and have been reported several times before with metal-on-metal epitaxy [42–44].

A closer inspection of the coverage dependence, especially at higher deposition temperatures, reveals a whole series of different structural features until the Re–Ag lattice misfit is overcome and the Ag film can grow with its characteristic inherent lattice parameters. All these features cannot only be seen with the STM, but show up also in the respective LEED patterns. Their description and discussion will be subject of the following section.

3.3. Ag deposition at elevated temperatures ($400 < T < 600$ K)

3.3.1. Low-energy electron diffraction

LEED patterns taken from Ag deposits grown at $T \geq 400$ K actually exhibit only a little diffuse background and damping of the Re(1 × 1) LEED intensity in the coverage range up to the monolayer; no "extra" spots are formed. This can be taken as a clear hint that the Ag atoms form an adlayer with the same periodicity as the Re substrate, whereby the overall concentration of diffuse scattering centers (i.e. the frayed edges of the Ag islands) is significantly reduced compared to the 300 K situation. This could be interpreted as strong evidence for pseudomorphic growth of the Ag adlayer. However, since the metallic radius of Ag is ~4.7% larger than that of Re, pseudomorphic growth must imply a marked compression of the Ag atoms in the respective layer. This compression will cause an additional increase in the mechanical strain energy as the second and third Ag layers grow on top. As a result, a special morphology is induced, namely misfit dislocation domains, as mentioned in Section 3.2. However, compared to the 300 K films, the structural features are more pronounced and better imaged at 400 K, and particularly at 600 K, deposition temperature.

The deposition of ~2 monolayers of Ag at 400 K changes the LEED patterns as depicted in Fig. 5a. The six hexagonal Re(1 × 1) spots exhibit (Ag-induced) concentric satellites inside the hexagon. We recall that the same pattern (although of worse quality) also appeared after deposition of $\Theta > 4$ Ag monolayers at 300 K. Patterns of this kind indicate a superposition of diffraction contributions of two independent crystal lattices with slightly different lattice parameters and provide evidence of both epitaxial growth and long-range order within the overlayer. From the LEED pattern we can deduce the lattice vector of the Ag layer by taking the reciprocal Re lattice vector as a calibration length for $a_{Re} = 2.76$ Å. Within the limits of accuracy we then arrive at a value for the silver(111) lattice parameter of $a_{Ag} = 2.92 \pm 0.05$ Å, which corresponds, within the limits of accuracy, to the Ag bulk value of 2.88 Å.

Interestingly, the deposition of still larger amounts of Ag ($\Theta > 2$ ML) leads to a diffraction pattern (shown in Fig. 5b) in which the "new" Ag-induced LEED spots of Fig. 5a are symmetrically surrounded by six tiny, but fairly sharp, "extra" spots with hexagonal symmetry, with the superstructure lattice vector not noticeably being rotated with respect to the substrate lattice. First- and second-order diffraction maxima are clearly visible as proven by the inset of Fig. 5b.

We only mention here that similar LEED patterns were described for (111) oriented Cu [1] and Au films [7] on Ru(0001), while for Ag(111) films deposited on Ru(0001) it is true that tiny hexagons around each substrate spot were also reported, but they were rotated by 30° with respect to the lattice vector of the hexagonal Ru substrate mesh [9,45]. Fig. 5b may either represent LEED coincidence patterns which originate from two extended homogeneous monolayer or bilayer films each with hexagonal long-range order, but slightly different (and differently directed) lattice vectors, or (as in our case) by a superposition of diffractive contributions of a plain Ag(111) lattice and a second,

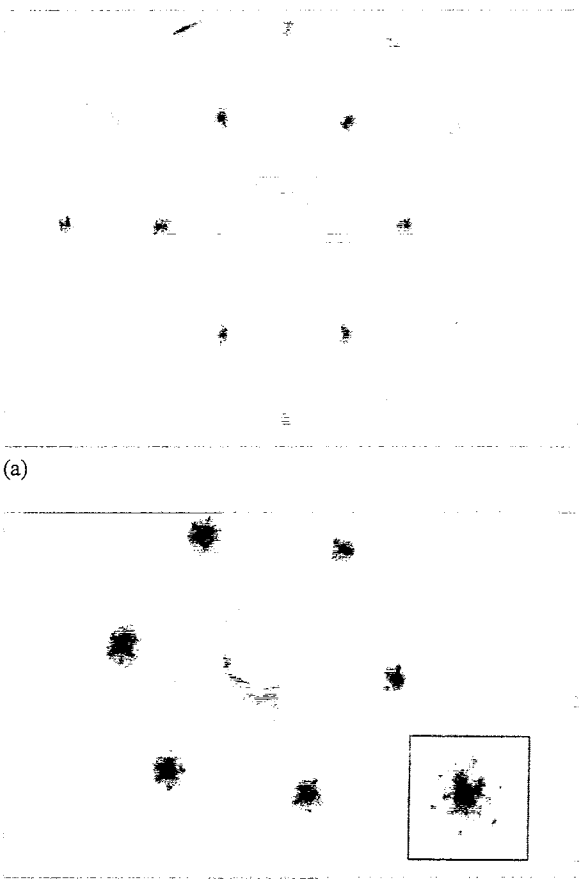

(a)

(b)

Fig. 5. (a) LEED pattern obtained from an ~2 ML thick Ag film deposited onto Re(0001) at 400 K and annealed for 5 min to 500 K. The two hexagonal spot systems due to Re (outer spots) and Ag (inner spots) indicate clear epitaxial growth of the Ag deposit. For clarity, the black-and-white contrast has been inverted. The electron energy was 131 eV. (b) LEED pattern of a 2 ML Ag film deposited at 400 K and annealed for 10 min at 750 K. The Re(1 × 1) reflexes are surrounded by tiny "extra" spots with hexagonal symmetry, indicating a clear coincidence structure between the first Ag layer and the misfit dislocation domain structure. Only the first- and second-order diffraction maxima are recognizable, as the inset of a single integer-order spot and its surrounding shows. For better visibility, the black-and-white contrast has been inverted. Electron energy $E = 95$ eV.

likewise hexagonal, periodic structure with a much larger unit mesh. The absence of higher-order diffraction maxima in the LEED pattern of Fig. 5b has to do with structural imperfections, poor resolution of the LEED device and systematic extinctions due to phase relations. At any rate, the lattice vector relation between the small and the large hexagons (the latter one being associated with the Ag(1 × 1) lattice) suggests a common period length (where the two coincidence lattices "lock in") of approximately 18 Re–Re distances, i.e. 50 Å.

The principal LEED pattern of Fig. 5b is retained up to the deposition of at least 6 Ag monolayers. At even larger coverages the tiny "extra" spots gradually disappear and we are left with the typical hexagonal (1 × 1) LEED pattern that is expected for an epitactic Ag film with (111) orientation.

3.3.2. *Scanning tunneling microscopy*

3.3.2.1. Nucleation and growth at $T \geq 400$ K. The higher mobility of the Ag atoms at elevated temperatures is reflected in the STM image presented in Fig. 6. It shows a detail of an Re surface region with a fairly high density of monoatomic steps of different width ranging from ~50 to 500 Å. Note that the direction of the steps is parallel to the $[\bar{1}\bar{1}20]$ direction of the Re substrate, i.e. follows the closely-packed Re rows of the (0001) surface. The silver coverage was ~0.1 nominal monolayers and it can be seen quite clearly that (i) the Ag atoms nucleate *exclusively at step edges*, (ii) the Ag nuclei start to form *only at every second step* and (iii) the nuclei consist of single Ag layers (we observe about the same, somewhat increased, imaging height as before with the 300 K deposits).

The surprising fact that Ag nuclei form only at every second step edge (provided that these edges are parallel to one of the densely packed rows of the Re substrate) underlines the high mobility of the Ag atoms that enables them to overcome the potential energy barriers at the terrace boundaries and to reach the most favorable binding ("adsorption") sites. Due to the particular stacking sequence of the hcp lattice, monoatomic steps of the (0001) surface provide, alternatingly, threefold adsorption sites with fcc and hcp symmetry on adjacent ter-

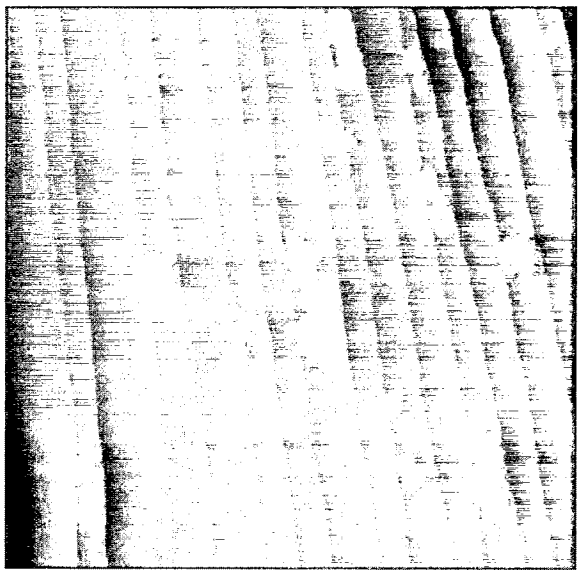

Fig. 6. STM image showing a detail (420 Å × 420 Å) of an Re surface region with a fairly high density of monoatomic steps of similar width of about 20–40 Å acting as nucleation centers for the Ag atoms which were deposited at 400 K to a nominal coverage of $\Theta = 0.1$. The (monoatomic) steps are parallel to the closely-packed rows of Re(0001); clearly, the Ag nuclei form only at every second step ($I = 0.12$ nA; $U = 150$ mV).

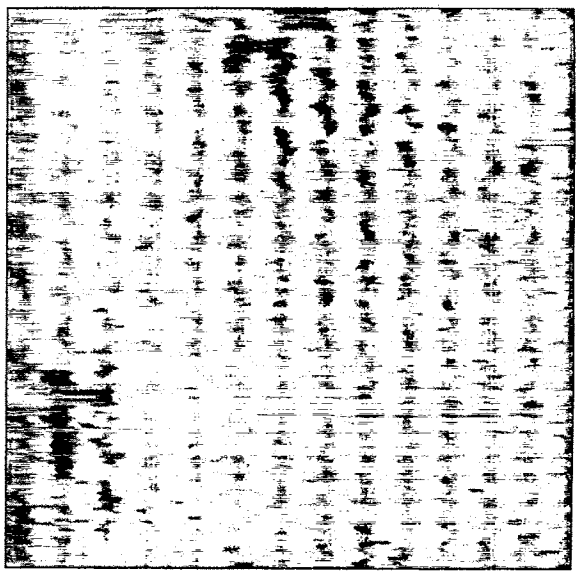

Fig. 7. STM image (39 Å × 39 Å) with atomic resolution obtained from a nominal coverage of 0.2 ML at 600 K. In the detail depicted in Fig. 7 a complete Ag monolayer was imaged showing the clear hexagonal symmetry with an Ag–Ag distance of ~2.8 Å. The monolayer film does not exhibit a corrugation, which may be taken as evidence of its pseudomorphic character ($I = 2.58$ nA; $U = 10$ mV).

races, and obviously the Ag atoms prefer one type of these sites for adsorption (which is very likely a hcp site because in this site the Ag atom can adsorb in a (111) microfacet, whereas occupation of an fcc site would lead to adsorption in a (100) microfacet with a somewhat reduced coordination). A similar behavior was found recently also for the Co/Re(0001) system [25,26] and the Co/Cu(111) system [46].

3.3.2.2. The structure of the first Ag monolayer. As the Ag coverage is increased and/or the temperature still somewhat raised to 600 K, the films become more compact due to enhanced diffusion processes. In this case it is possible to obtain STM images with atomic resolution and an example is presented in Fig. 7 for an Re surface covered with a complete Ag monolayer. Two observations deserve attention. First, the Ag film exhibits a clear hexagonal symmetry with (approximate) interatomic Ag–Ag distances of $\sim 2.8 \pm 0.1$ Å. Second, the film is absolutely flat, there is no indication of any periodic buckling. While the measured Ag–Ag distance of 2.8 Å does not allow a decision as to whether the film possesses the Re or the Ag lattice parameter and, hence, cannot confirm or rule out its pseudomorphic nature, the second observation of a *flat* film is more revealing and strongly suggests pseudomorphism of the Ag monolayer for the following reason. An Ag(111) film (with the Ag lattice constant) deposited on top of the Re surface would definitely exhibit a corrugation with an approximate period length of $p = 22 \times d_{Ag} = 23 \times d_{Re} \approx 63$ Å (with $d_{Ag} = 2.88$ Å and $d_{Re} = 2.76$ Å) since this is the repetition period for any kind of adsorption site (for example, an atop site) if the two undistorted hexagonal lattices of Ag and Re are put on top of each other (unrotated and parallel to the $[\bar{1}\bar{1}20]$ direction). In this hard sphere model an atop site causes an elevation, whereas the threefold hollow site (which exhibits the same repetition period but is phase-shifted by $p/2$) causes a depression. In other words, a *non-buckled smooth Ag film* can only exist if the two lattices are *perfectly*

congruent. This, however, requires that the Ag lattice must shrink to the dimensions of the Re host substrate as is suggested by our data.

At this point we expand somewhat on the "chemisorption" problem of Ag on Re(0001). Apparently, the energetics of this chemisorptive interaction must provide a certain "surplus" to compress the Ag adlayer to the dimensions of the Re(0001) surface, i.e. the density of the Ag film must increase by $\sim 8.9\%$ compared to an Ag(111) surface. It is not unreasonable to rationalize respective effects with heteroepitactic systems, which often exhibit such a strong chemical interaction between guest and host atoms that a considerable charge transfer takes place between the different atoms, resulting in an apparent shrinking of the "physical" size of the adatom, fairly independent of the substrate surface orientation, until the atomic diameters of host and guest atoms no longer deviate from one another and pseudomorphism occurs. Accordingly, such phenomena have been reported, especially for adsorption of alkali metals on noble metal surfaces [47,48], where the adsorbed alkali metal atoms reached a fairly ionic state by donating charge to the substrate.

However, we must consider the Ag-on-Re system a typical exponent of a *more weakly* interacting system. The two elements possess similar electronegativities (Pauling electronegativities of Ag and Re are $x_{Ag} \approx x_{Re} \approx 1.9$ [49]) and a massive chemically motivated charge transfer is rather less likely. The fact that the two metals are immiscible in the bulk also underlines the lack of chemical affinity. Accordingly, recent TDS measurements performed with Ag/Re(0001) [28] clearly showed that the specific interaction energies between Ag–Re and Ag–Ag are quite similar, a fact which is corroborated by X-ray photoelectron spectra which do not exhibit measurable core-level shifts of Ag and Re. In view of these results it is remarkable that quantitative work function change measurements revealed a non-negligible charge transfer from the Ag atoms to the Re substrate [28], and our structural results, in which the first Ag layer grows pseudomorphically, suggest that the Ag–Re interaction potential wells are deep enough to not only "guide" the impinging Ag atoms to certain favorable growth directions but to also provide enough energy to compensate the two-dimensional strain that is built up in a pseudomorphic layer.

3.3.2.3. The structure of the Ag bilayer. We recall that the lateral strain energy of the pseudomorphic first layer is compensated by the lateral variation in the Ag–Re interaction energy. While this led, for the 300 K films, to a misfit dislocation domain structure in which the first 2 to 3 Ag layers did not lose their pseudomorphic character, the high-temperature films behave differently when the first pseudomorphic film becomes covered by subsequent Ag layers. The STM image (Fig. 8), which scans an area of 100 Å × 100 Å, was obtained from a bilayer film after deposition at 600 K. From the overall distribution of light and dark tones one can, first of all, recognize a large-scale undulation

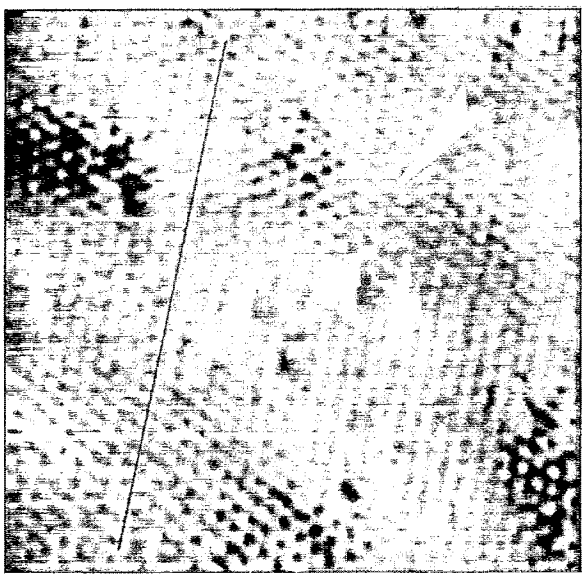

Fig. 8. Atomically resolved STM image (100 Å × 100 Å) of a bilayer Ag film deposited onto an Re(0001) substrate at $T=$ 600 K. From the distribution of light and dark tones one can deduce a large-scale undulation of the Ag film, with an approximate wavelength of $\sim$60–80 Å and a maximum corrugation amplitude of $\sim$0.2 Å. Note that the broad stripes change their direction (as indicated by the white arrow); the approximate bending angle is $\sim 120 \pm 20°$. The inspection of the atomically resolved film structure reveals that periodic displacements of Ag atoms occur perpendicular to the $[\bar{1}\bar{1}20]$ direction of the Re substrate (parallel to the dark guideline), indicating a uniaxial expansion of the surface lattice between fcc and hcp sites ($I=0.8$ nA; $U=13$ mV). See text for further details.

indicated by approximately three white–grey areas bordered by parallel darker regions. The approximate widths of these zones is 30–40 Å and their height difference amounts to ~0.2 Å. Interestingly, the broad stripes change their direction after every ~100 Å; the approximate angle between the directions is $\sim 120 \pm 20°$. This bending is indicated in Fig. 8 by a white arrow. Even more revealing is an inspection of the atomically resolved film structure. If one follows the direction of a selected string of individual Ag atoms in the $[\bar{1}\bar{1}20]$ direction of the Re substrate (as a guideline for the eye, we have drawn a sharp black line in this direction), one can clearly recognize periodic undulations in the densely packed rows of Ag atoms perpendicular to the $[\bar{1}\bar{1}20]$ direction, whereby the dislocation "amplitude" corresponds approximately to the distance between fcc and hcp sites of the Re(0001) substrate surface (1.6 Å) and the repetition (coincidence) period of 63 ± 3 Å to 24 ± 2 Re–Re distances. The respective elongation perpendicular to the $[\bar{1}\bar{1}20]$ direction causes a dilatation of the pseudomorphic lattice via a *uniaxial expansion* of the Ag–Ag distances. Macroscopically, this leads to a lower packing density of the Ag atoms and, hence, to a significantly reduced strain energy. Similar line structures have been reported also for the systems Ag/Ru(0001) [50,51] and Ag/Pt(111) [42]. All these systems exhibit, as does the Ag/Re(0001) system, a "positive" lattice misfit, which means that the deposit atoms are somewhat larger than the substrate atoms. A "negative" misfit is encountered with the system Cu/Ru(0001) [20,43] but also in this case bent line structures indicate uniaxial compressions. Finally, we note that the line structures observed with the reconstructed Au(111) [52–54] and Pt(111) surfaces [55] have been interpreted in quite an analogous manner, as will be discussed later.

Principally, the corrugation of uniaxially compressed structures can be explained by a simple hard-sphere model. However, if this model is applied also to uniaxially *expanded* structures, the height relation is inverted, an effect which is also seen in Fig. 8. The walls of adjacent domains (which represent the most elevated points) are imaged as *depressions*, although the Ag atoms there are adsorbed in bridge and not in hollow positions. At the same time, those areas where the Ag atoms are located in hollow sites are imaged as elevations; the opposite to the real-space situation. Despite this apparent height inversion in the STM imaging, the validity of the fcc→hcp site-transition model is also documented by the change of the domain-wall *direction* which occurs in a similar fashion as described previously for the reconstructed Au(111) surface. From studies by Chambliss et al. [56] it is well known that the "elbows" of the characteristic "herring-bone" or "chevron" domain-wall structure of this reconstructed surface induce so-called edge dislocations, because atoms must be removed as the wall turns. We underline that the respective dislocations occur also in our case of the Ag bilayer film but in a dark (low height level) and not in a light (increased height level) area. While in the largely magnified STM image of Fig. 8 this effect seems to be restricted to a single direction only, the turns of the dislocation lines after about 100 Å make sure that all three high-symmetry directions of the (0001) surface contribute, resulting in a homogeneous relaxation on the macroscopic scale.

3.3.2.4. The structure of 3 ML and 4 ML Ag films. In agreement with the LEED results (which revealed the complex pattern displayed in Fig. 5a) the Ag film exhibits a peculiar morphology, i.e. the surface consists of a fairly homogeneous network of elevations and depressions with appreciable long-range order. Fig. 9 illustrates the situation. Fig. 9a presents a 1030 Å × 1030 Å detail of a two-terrace region separated by a monoatomic step. On the higher terrace (the left part of the image) a two-monolayer film is depicted while on the lower terrace on the right-hand side a three-monolayer film has grown. Because of its very small corrugation (cf. Section 3.3.2.3) the uniaxially expanded bilayer film shows only vanishing contrast and appears to be homogeneous. However, for the *trilayer* film we clearly recognize the *network of lines with hexagonal symmetry*, with a significant height modulation imaged by the STM. This modulation and the hexagonal long-range symmetry can be nicely seen in the 150 Å × 150 Å detail of Fig. 9b (which does not represent an image with atomic resolution!); the "lattice constant" of this network is about 51 ± 4 Å ($\triangleq 18 \pm 2$ atomic Re–Re

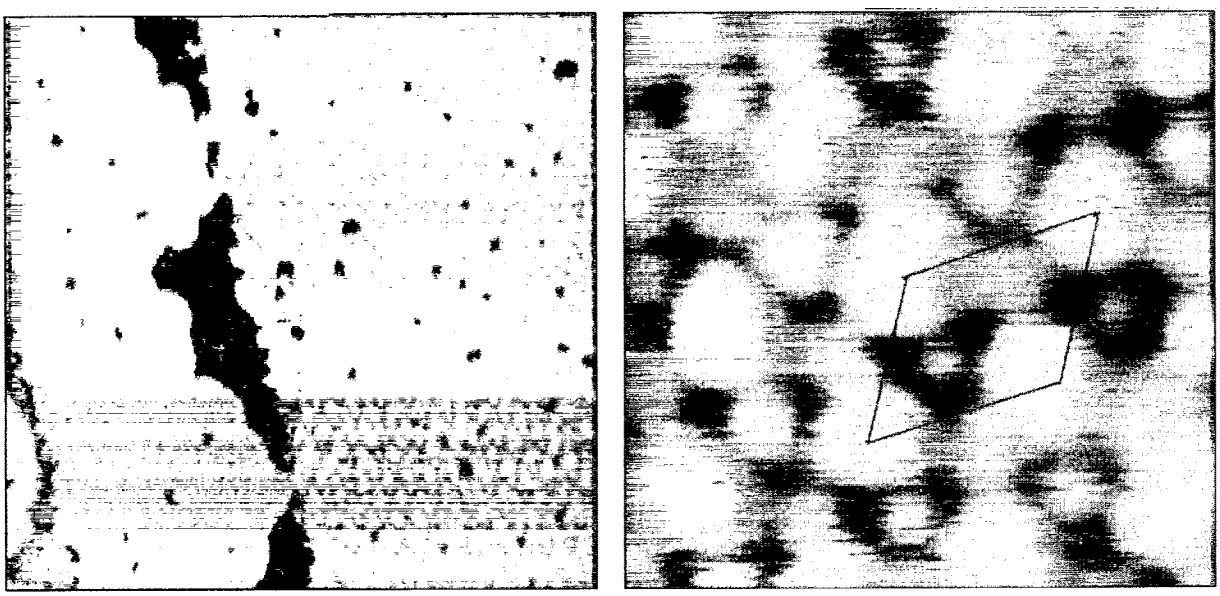

(a) (b)

Fig. 9. (a) 1030 Å × 1030 Å STM detail of a two (three) monolayer Ag film on Re(0001). Shown is a two-terrace region separated by a monoatomic step, the left part of the image consisting of a *two*-monolayer film, the right part of a *three*-monolayer Ag deposit. Both films exhibit a network of depression lines, which are hardly recognizable for the bilayer film (due to the comparatively small corrugation amplitude) but appear quite clearly for the three-layer film. It is believed that these periodic structures represent a moiré pattern formed by slightly relaxed (rotated) Ag(111) surface meshes ($I=0.21$ nA; $U=45$ mV). (b) Detail magnification (150 Å × 150 Å) of the trilayer Ag film of (a) illustrating the height modulation and the hexagonal long-range symmetry of the moiré pattern. Note that not individual atoms are imaged but rather elevations and depressions on the 50–100 Å scale. Indicated is the hexagonal unit mesh of the periodic structure which possesses a "lattice constant" of 51 ± 4 Å ($\approx 18\pm2$ atomic Re–Re distances). The maximum corrugation amplitude is ~0.8 Å ($I=0.24$ nA; $U=32$ mV).

distances), which agrees very well with the period lengths deduced from the complex LEED structure (Fig. 5b) mentioned in Section 3.3.1. The hexagonal unit cell indicated in Fig. 9b contains three maxima with different height levels, namely a single very bright maximum and two less intense elevations with lower (and mutually different) intensity. While the maximum corrugation amplitude amounts to ~0.8 Å, the height difference between the two less intense maxima is about 0.2 Å only. Although Fig. 9a suggests that the unit cells do not possess a *perfect* long-range periodicity (slight undulations and, hence, dislocations of the translation vectors occur frequently) we succeeded in obtaining the relatively complex LEED pattern of Fig. 5b mentioned above. At first sight, one might interpret the real-space structure of the trilayer Ag films as a moiré pattern caused by a superposition (and possibly an additional rotation) of fairly rigid Ag lattices each possessing a slightly different lattice constant. More likely, however, we simply observe the continuation of the trigonal domain-wall structure in the third layer. Similar domain-wall structures have been reported for the Ag-on-Pt(111) system and are discussed in detail by Brune et al. [42].

As the thickness of the Ag deposit reaches three and four layers, the gross features persist in that both the complex LEED pattern and a real-space network with hexagonal symmetry can still be seen, although some changes occur in detail. This is illustrated in Fig. 10a, which reproduces again a region (660 Å × 660 Å) with two adjacent terraces, the left one covered with a three Ag monolayer and the right one with a four-layer silver film. Even at a first glance, the overall fine structure of

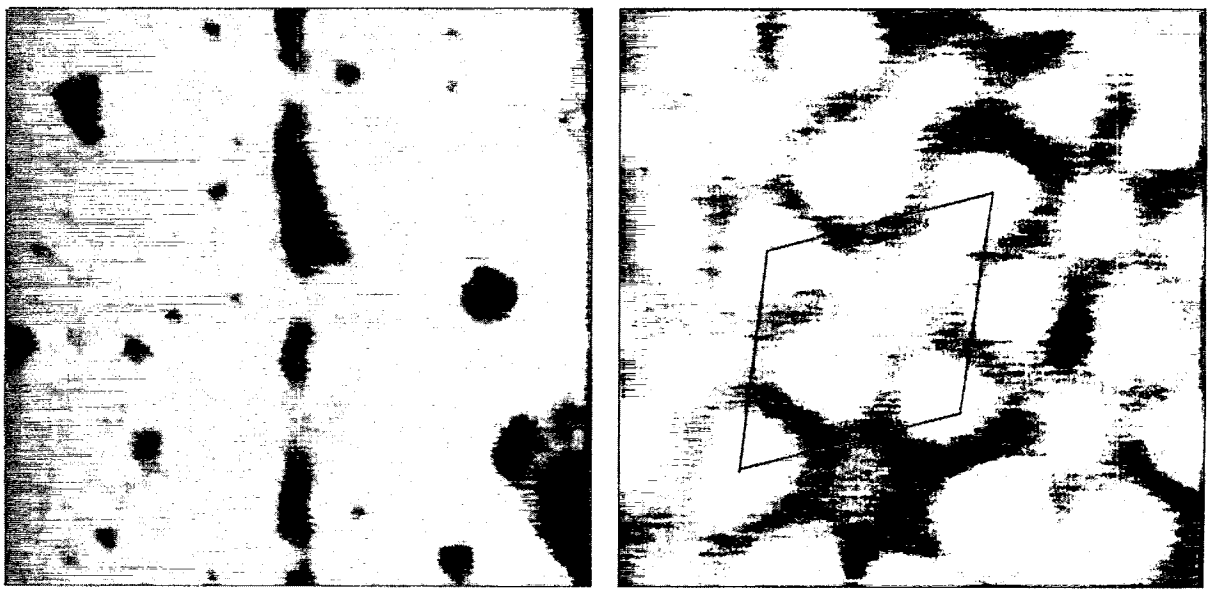

(a) (b)

Fig. 10. (a) 660 Å × 660 Å STM detail of a three (four) monolayer Ag film on Re (0001). As in Fig. 9a we reproduce a two-terrace region separated by a monoatomic step, the left part of the image consisting of a *three*-monolayer, the right part of a *four*-monolayer Ag film prepared at 600 K. Again, moiré patterns appear, with the overall corrugation amplitude of the four-layer film being somewhat reduced as compared to the trilayer film ($I=0.15$ nA; $U=61$ mV). (b) Further magnification (130 Å × 130 Å) of the four-layer Ag film of (a) illustrating the hexagonal symmetry of the superstructure (which appears to be of the honeycomb type). Again indicated is the unit mesh of the periodic structure which is of about the same size (50 Å) as for the three-layer film but exhibits different internal height modulations which give the (incorrect) impression of a smaller size of the unit cell. The maximum corrugation amplitude is merely ~0.6 Å ($I=0.24$ nA; $U=32$ mV).

the two regions appears to be different: the three-layer film on the left exhibits a fairly coarse mesh, while the four-layer film on the right seems to consist of narrower meshes, thus suggesting a smaller unit cell. However, as the larger magnification (imaged area 130 Å × 130 Å) reproduced in Fig. 10b proves, there appear to be slightly different intensity modulations of the interior of the non-primitive unit mesh only (indicated by black lines), in that merely two maxima of different height (height level difference ~0.6 Å) can be distinguished. Hence, it is suggested that the overall symmetry is of the honeycomb type, which causes the aforementioned impression of a smaller unit cell for the four-layer Ag film. The net result is that the overall corrugation amplitude of this four-layer film is further reduced as compared to the tri- or the bilayer Ag film, and Ag films of this thickness prepared at a temperature $T \geq 400$ K have almost completely undergone isotropic relaxation to the Ag(111) lattice plane. As for the trilayer film, the long-range periodicity is not perfectly good but still sufficient to allow the observation of a LEED superstructure. It is, however, somewhat difficult to discover and analyze the changes of the symmetry and the period length suggested by the STM data in the LEED patterns due to their limited resolution and the fairly large diffuse background which neither allows a quantitative determination of the lengths of the reciprocal vectors nor a clear-cut statement as regards the spot symmetry.

The reason for the formation of different moiré patterns, depending on whether 3 or 4 Ag monolayers are considered, may be seen in a (layer-dependent) minimization of the surface free energy, which can involve different rotation angles and/or undulations of the two superimposed surface

lattices. This can easily be demonstrated by a superposition of two rigid hexagonal surface lattices, which are rotated by different (small) angles with respect to each other. This procedure yields nice moiré patterns with hexagonal symmetry but different long-range periodicity.

Finally, we note that an increase in the number of deposited Ag layers to beyond ~ 6 causes all moiré patterns to disappear, indicating that the films become very flat and smooth and are practically identical with genuine (111) Ag layers. (Nevertheless, a structural change in the lattice(s) near the Re–Ag interface must still exist.)

All in all, the overall Ag film morphology, i.e. the structural features of the individual layers (which, however, cannot be considered independently) appear to result from a critical interplay between kinetics and thermodynamics; this could be shown for both the formation of Ag islands in the submonolayer range and the growth of complete Ag layers. As pointed out by Bauer [57], there is a clear-cut thermodynamical condition that will lead to strictly two-dimensional, i.e. layered, growth. The specific surface free energy of the host surface, γ_h should exceed the sum of the specific surface free energy of the deposited guest material, γ_g, and the interfacial energy, γ_i, between the two materials. (Continuous layered growth requires that this energy balance holds for every new deposited Ag layer on top.) For the Ag-on-Re system we have $\gamma_h \equiv \gamma_{Re} \approx 3.6\ J\ cm^{-2}$ and $\gamma_g \equiv \gamma_{Ag} \approx 1.3\ J\ cm^{-2}$ [58]; unfortunately, the interfacial energy γ_i is not known but we may safely assume that it is small due to the repeatedly mentioned lack of chemical affinity between Ag and Re. Accordingly, one would expect, if thermodynamics *alone* is the regulating principle, a genuine layer-by-layer growth with rather compact Ag films, simply because a spreading of the Ag atoms on the Re surface can help to reduce its comparatively high surface free energy. The fact that layered growth finally occurs in an almost ideal manner, especially for the high-temperature films, demonstrates the importance of thermodynamics in the present case. By contrast, the morphology of the 300 K films is rather dominated by kinetics. The reason why complete layers are nevertheless formed at least for the first and second Ag monolayers is a significantly reduced Schwoebel barrier for diffusion over step edges, which supports appreciable interlayer mass transport.

4. Conclusions

In summary, we found the Ag-on-Re(0001) system a good example for a very rapid adaptation of two different lattices. All our results indicate that (despite the appreciable lattice misfit between Ag and Re) the matching to the bulk silver lattice is accomplished within one or two layers, whereby the first Ag monolayer grows pseudomorphically with the Re lattice parameter while thicker films relax first by a uniaxial expansion (bilayer films) and by (slight) three-dimensional lattice relaxation and rotation, leading to moiré patterns for the tri- and tetralayer films. After deposition of ~ 6 monolayers the film is sufficiently relaxed that it can be considered part of a genuine silver (111) crystal.

Acknowledgements

We are grateful to K. Schubert and R. Cames for technical assistance. This work was financially supported by the Deutsche Forschungsgemeinschaft through SFB 290.

References

[1] K. Christmann, G. Ertl and H. Shimizu, J. Catal. 61 (1980) 397; 412.
[2] J.C. Vickerman and K. Christmann, Surf. Sci. 120 (1982) 1.
[3] K. Christmann and G. Ertl, J. Mol. Catal. 25 (1984) 31.
[4] J.E. Houston, C.H.F. Peden, D.S. Blair and D.W. Goodman, Surf. Sci. 167 (1986) 427.
[5] K.S. Kim, J.H. Sinfelt, S. Eder, K. Markert and K. Wandelt, J. Phys. Chem. 91 (1987) 2337.
[6] F.M. Hoffmann and J. Paul, J. Chem. Phys. 84 (1987) 2990.
[7] Chr. Harendt, K. Christmann, W. Hirschwald and J.C. Vickerman, Surf. Sci. 165 (1986) 413.
[8] A. Jablonski, S. Eder and K. Wandelt, Appl. Surf. Sci. 22/23 (1985) 305.
[9] B. Konrad, D. Rieger, R.D. Schnell, W. Steinmann and K. Wandelt, BESSY-Jahresbericht (1985) 186.

[10] J.H. Sinfelt, Acc. Chem. Res. 10 (1977) 15.
[11] J.H. Sinfelt, Bimetallic Catalysts (Wiley, New York, 1983).
[12] C.T. Campbell, Annu. Rev. Phys. Chem. 41 (1990) 775.
[13] M. Hansen, Constitution of Binary Alloys (McGraw-Hill, New York, 1958).
[14] H. Asonen, C. Barnes, A. Salokatve and A. Vuoristo, Appl. Surf. Sci. 22/23 (1985) 556.
[15] K.H. Frank, R. Dudde, J.H. Sagner and W. Eberhardt, Phys. Rev. B 39 (1989) 940.
[16] Y. Wu, H.-S. Tao, E. Garfunkel, T.E. Madey and N.D. Shinn, Surf. Sci. 336 (1995) 123.
[17] E. Kopatzki, H.G. Keck, I.D. Baikie, J.A. Meyer and R.J. Behm, Surf. Sci. 345 (1996) L11.
[18] D.R. Short, S.M. Khalid, J.R. Katzer and M.J. Kelley, J. Catal. 72 (1981) 288.
[19] P. van der Plank and W.M.H. Sachtler, J. Catal. 12 (1968) 35.
[20] G.O. Pötschke and R.J. Behm, Phys. Rev. B 44 (1991) 1442.
[21] R.Q. Hwang, J. Schröder, C. Günther and R.J. Behm, Phys. Rev. Lett. 67 (1991) 3279.
[22] G.O. Pötschke, J. Schröder, C. Günther, R.Q. Hwang and R.J. Behm, Surf. Sci. 251/252 (1991) 592.
[23] R.Q. Hwang, C. Günther, J. Schröder, S. Günther, E. Kopatzki and R.J. Behm, J. Vac. Sci. Technol. A 10 (1992) 1970.
[24] J. Wintterlin and R.J. Behm, in Scanning Tunneling Microscopy I, Eds. H.J. Güntherodt and R. Wiesendanger, Springer Series in Surface Science, 2nd ed. (Springer, Berlin/New York, 1991) p. 37.
[25] M. Parschau and K. Christmann, Ber. Bunsenges. Phys. Chemie 99 (1995) 1376.
[26] M. Parschau, Ph.D. thesis, Free University, Berlin, 1996.
[27] H. Röder, R. Schuster, H. Brune and K. Kern, Phys. Rev. Lett. 71 (1993) 2086.
[28] D. Schlatterbeck, M. Parschau and K. Christmann, to be published.
[29] D.D. Chambliss and R.J. Wilson, J. Vac. Sci. Technol. B 9 (1991) 928.
[30] H. Röder, K. Bromann, H. Brune and K. Kern, Phys. Rev. Lett. 74 (1995) 3217.
[31] T.A. Witten and L.M. Sander, Phys. Rev. Lett. 47 (1981) 1400.
[32] T.A. Witten and L.M. Sander, Phys. Rev. B 27 (1983) 5686.
[33] P. Meakin, Phys. Rev. A 27 (1983) 1495.
[34] P. Meakin, Phys. Rev. Lett. 51 (1983) 1119.
[35] R.Q. Hwang, J. Schröder, C. Günther and R.J. Behm, Phys. Rev. Lett. 67 (1991) 3279.
[36] H. Röder, H. Brune, J. Bucher and K. Kern, Surf. Sci. 298 (1993) 121.
[37] Y.W. Mo and F.J. Himpsel, Phys. Rev. B 50 (1994) 7868.
[38] H. Bethge, D. Heuer, Ch. Jensen, K. Reshöft and U. Köhler, Surf. Sci. 331–333 (1995) 878.
[39] R.L. Schwoebel, J. Appl. Phys. 40 (1969) 614.
[40] K. Bromann, H. Brune, H. Röder and K. Kern, Phys. Rev. Lett. 75 (1995) 677.
[41] J. Vrijmoeth, H.A. van der Vegt, J.A. Meyer, E. Vlieg and R.J. Behm, Phys. Rev. Lett. 72 (1994) 3843.
[42] H. Brune, H. Röder, C. Boragno and K. Kern, Phys. Rev. B 49 (1994) 2997.
[43] C. Günther, J. Vrijmoeth, R.Q. Hwang and R.J. Behm, Phys. Rev. Lett. 74 (1995) 754.
[44] J.A. Meyer, P. Schmidt and R.J. Behm, Phys. Rev. Lett. 74 (1995) 3864.
[45] B. Konrad, F.J. Himpsel, W. Steinmann and K. Wandelt, Proc. Int. Conf. on Structure Determination by LEED and other Methods, Erlangen (1985) p. 109.
[46] J. de la Figuera, J.E. Pristo, C. Ocal and R. Miranda, Phys. Rev. B 47 (1993) 13043.
[47] D.K. Flynn-Sanders, K.D. Jamison, J.V. Barth, J. Wintterlin, P.A. Thiel, G. Ertl and R.J. Behm, Surf. Sci. 253 (1991) 270.
[48] A. Neumann, S.L.M. Schröder and K. Christmann, Phys. Rev. B 51 (1995) 17007.
[49] L. Pauling, Die Natur der chemischen Bindung, 2nd ed. (Verlag Chemie, Weinheim, 1964) p. 475.
[50] R. Hwang, J. Hamilton, L. Stevens and S. Foiles, Phys. Rev. Lett. 75 (1995) 4242.
[51] J. Stevens and R. Hwang, Phys. Rev. Lett. 74 (1995) 2078.
[52] C. Wöll, S. Chiang, R.J. Wilson and P.H. Lippel, Phys. Rev. B 39 (1989) 7988.
[53] J.V. Barth, H. Brune, G. Ertl and R.J. Behm, Phys. Rev. B 42 (1990) 9307.
[54] U. Harten, A. Lahee, J.P. Toennies and C. Wöll, Phys. Rev. Lett. 54 (1985) 2619.
[55] M. Bott, M. Hohage, T. Michely and G. Comsa, Phys. Rev. Lett. 70 (1993) 6609.
[56] D.D. Chambliss, R.J. Wilson and S. Chiang, J. Vac. Sci. Technol. B 9 (1991) 933.
[57] E. Bauer, Ber. Bunsenges. Phys. Chem. 95 (1991) 1315.
[58] A.R. Miedema and J.W. Dorleijn, Surf. Sci. 95 (1980) 447.